Sol-gel processing of alkoxysilyl-substituted nickel complexes for the preparation of highly dispersed nickel in silica†

Gregor Trimmel, Christian Lembacher, Guido Kickelbick and Ulrich Schubert*

Institute of Materials Chemistry, Vienna University of Technology, Getreidemarkt 9/165, A-1060 Wien, Austria

Received (in Strasbourg, France) 6th November 2001, Accepted 31st January 2002
First published as an Advance Article on the web

Nanocomposites containing nickel nanoparticles in silica were obtained by sol-gel processing of $Ni(NO_3)_2$, $Ni(OAc)_2$ (OAc = acetate), $NiCl_2$, or Ni(acac)$_2$ (acac = acetylacetonate), a complexing silane [$(EtO)_3Si(CH_2)_3NHCH_2CH_2NH_2$, $(EtO)_3Si(CH_2)_3NH_2$ or $(RO)_3Si(CH_2)_3NHCH_2CH_2NHCH_2CH_2NH_2$] and $Si(OEt)_4$, followed by calcination of the metal-complex-containing xerogels in air and reduction in hydrogen. Two types of nanocomposite materials were prepared, both containing about 8–8.5 wt % of elemental nickel: (i) Ni/SiO_2 nanocomposite powders in which the silica matrix is mainly formed from $Si(OR)_4$, and (ii) Ni particles on pre-formed silica spheres. The latter were prepared by impregnating silica spheres with sols from the particular complexing silane–nickel salt combination followed by calcination and reduction. In both types of materials, the average nickel particle size is influenced by the composition of the precursor mixture, particularly the counter-ion of the employed nickel salt. The smallest particles (diameter below 3 nm) were obtained from $Ni(NO_3)_2$ [and $Ni(OAc)_2$ for the powders], while the use of Ni(acac)$_2$ and $NiCl_2$ resulted in larger nickel particles. The variation of the nickel particle diameters was much larger for the powders than for the impregnated spheres.

Sol-gel processing allows the preparation of non-agglomerated metal oxide or metal nanoparticles within a silica matrix with particularly narrow particle size distributions and adjustable metal loading, if the metal precursor is tethered to the gel network during sol-gel processing. The dispersed metals are prepared by a four-step procedure, as previously reported.[1–3] In the first step metal complexes of the type $[(RO)_3Si(CH_2)_n\text{-}A]_nMX_m$ are formed *in situ* upon reaction of a metal salt (MX_m) with a complexing silane $(RO)_3Si(CH_2)_nA$, where A represents an organic group capable of coordinating metal ions, mostly nitrogen-donor groups. When the resulting complexes $[(RO)_3Si(CH_2)_nA]_nMX_m$ are processed by the sol-gel method in the second step, the metal coordination is retained, and the metal complexes are tethered to the silicate matrix *via* the $(CH_2)_nSiO_{3/2}$ groups. The metal loading can be adjusted by adding $Si(OR)_4$ to the precursor solution. The resulting metal-complex-containing gels with the idealized composition $[O_{3/2}\text{-}Si(CH_2)_nA]_nMX_m{\cdot}x\ SiO_2$ are then dried and heated in air to oxidize/pyrolyze all organic moieties. Nano-sized metal oxide particles [*i.e.*, the nanocomposites $MO_y{\cdot}(x+n)SiO_2$] are formed due to the molecular dispersion of the metal ions in the sol-gel step. If one wants to get carbon-free composites, the oxidation temperature has to be high enough to ensure complete oxidation of all organic components, but should not be higher than necessary to avoid excessive sintering of the metal particles. In the final step, the metal oxide particles are reduced by hydrogen, and the composites $M{\cdot}(x+n)SiO_2$ are obtained.

The average metal particle size is metal-dependent, but the particle size distributions are very narrow. This method has found application for the preparation of a variety of nanocomposites, in which single-metal or alloy particles are embedded in a silica matrix. Apart from composite powders, highly dispersed metals on solid supports can also be prepared. For this application, the metal-complex-containing sols obtained after the first step were sprayed onto the supports and then converted into metal particles in silica.[3] Metal-doped aerogels were obtained by supercritical drying of the metal-complex-containing gels prior to calcination and reduction.[4]

In previous studies we have mainly investigated how the textural properties of the obtained nanocomposites[5] and the metal particle size for Cu/Ni and Pt particles[2,3] are influenced by the reaction conditions, particularly the oxidation conditions, but also on the chemical composition of the precursor mixture. For example, the average metal particle size in Pt/SiO_2 can be varied by a factor of more than five for a given set of reaction parameters just by using different platinum salts and alkoxysilanes $(RO)_3Si(CH_2)_nA$ with different groups A.[3]

In the present paper we extend these studies to nickel/SiO_2 nanocomposites, which are interesting because of their catalytic, magnetic and electric properties. Because of the less noble character of the metal, the stronger metal-matrix interactions[6] and the easy formation of volatile metal carbonyls, nickel/silica nanocomposites are more difficult to optimize than the corresponding platinum/silica systems. Highly dispersed nickel in silica is highly interesting as a catalyst for hydrogenation, dehydrogenation or hydrogenolysis reactions. The metal particle size often plays a crucial role for the catalytic activity. For example, the hydrogenolysis rate of ethane was increased by a factor of 10 when the particle size was decreased from 22 to 2.5 nm.[7]

Results and discussion

According to our earlier studies, three parameters of the precursor mixture are relevant to the final materials properties: (*i*) the counter-ion of the metal ion, (*ii*) the complexing group

† Electronic supplementary information (ESI) available: Tables S1–S5 giving additional analytical data as described in the text and the exact quantities for the syntheses. See http://www.rsc.org/suppdata/nj/b1/b110612k/

Table 1 Color and appearance of the xerogels after drying

Series	Silane	$Ni(NO_3)_2$	$Ni(OAc)_2$	$NiCl_2$	$Ni(acac)_2$
A	1 AEAPTS	Light green powder	Turquoise solid	Green powder	Yellow solid
B	2 AEAPTS	Turquoise powder	Blue solid	Blue powder	Yellow solid
C	3 AEAPTS	Light blue powder	Blue solid	Blue powder	Yellow solid
D	2 APS	Light green powder	Light green powder	Light green powder	Yellow powder
E	1 TRIAMIN	Light blue powder	Turquoise solid	Light green powder	Brown solid

Table 2 Absorption maxima λ_{max} (nm) in the UV-Vis spectra of the xerogels (320–800 nm)

Series	Silane	$Ni(NO_3)_2$	$Ni(OAc)_2$	$NiCl_2$	$Ni(acac)_2$
A	1 AEAPTS	381, 645	387, 640	405, 671	508, 739
B	2 AEAPTS	563	597	371, 597	—
C	3 AEAPTS	350, 569	360, 576	360, 574	510, 711
D	2 APS	390, 667	390, 664	407, 701	500
E	1 TRIAMIN	372, 600	376, 613	375, 621	728

A of the silane $(RO)_3Si(CH_2)_3A$, and (*iii*) the metal:$(RO)_3Si(CH_2)_3A$ ratio. The following precursors were used in this study: $Ni(NO_3)_2$, $Ni(OAc)_2$ (OAc = acetate), $NiCl_2$, and $Ni(acac)_2$ (acac = acetylacetonate) as the metal compounds, and 1–3 molar equiv of 3-(2-aminoethylamino)propyltriethoxysilane (AEAPTS), 2 molar equiv of aminopropyltriethoxysilane (APS), or 1 molar equiv of (3-trimethoxysilylpropyl)diethylentriamine (TRIAMIN) as the complexing silanes (Table 1).

In the following, the samples will be designated as NO(X), Ac(X), Cl(X) or Acac(X), where NO represents nickel nitrate, Ac the acetate, Cl the chloride and Acac the acetylacetonate, and X is the series label defined in Table 1. The letters x, o and r refer to the xerogels (x), the calcined samples (o) or the reduced samples (r), respectively [for example, NO(C)x is a xerogel prepared from $Ni(NO_3)_2$ and 3 equiv of AEAPTS as the complexing silane (series C)].

Metal-complex-containing xerogels

When the amino-substituted silanes were added to ethanolic suspensions of the metal salts, the chloride, acetate and nitrate dissolved at room temperature, while the suspension of the acetylacetonate had to be heated for several hours. The solutions then had the typical color of the corresponding amine complexes (see Table 1). Since hydrated salts were used (except the acac derivative), it must be assumed that some prehydrolysis took place during this stage. To get reproducible results, water-free, not denatured ethanol was used. Due to the large excess of solvent used (relative to the alkoxysilanes), even small amounts of water in the solvent result in additional but uncontrolled premature hydrolysis reactions. After complexation of the metal ions by the amino-substituted alkoxysilanes, aqueous NH_4OH was added to the solution for further prehydrolysis, and $Si(OEt)_4$ (TEOS) after 15 min. The TEOS proportion was chosen so that the final composites had a theoretical nickel content of 8.5 wt % (9.5 mol %). The obtained gels were aged at 70 °C for 3 days and then dried at 80 °C/0.1 Torr until no further mass loss occurred.

Gels were only obtained when nickel acetate or acetylacetonate was reacted with AEAPTS or TRIAMIN. In all other cases, suspensions or pulp-like masses were obtained instead of gels. Some of the samples were obtained as fine powders after drying, and others as solid masses (see Table 1).

We have previously shown[1] that the reaction of $Ni(OAc)_2$ with 1–3 equiv of AEAPTS results in the formation of metal complexes that have nearly the same UV spectra as the corresponding ethylene diamine (en) or 2,3-diaminobutane (dbn) complexes ($[Ni(dbn)]^{2+}$ $\lambda_{max} = 372$, 623 nm; $[Ni(dbn)_3]^{2+}$ $\lambda_{max} = 353$, 557 nm).[8] Very similar UV spectra were obtained when ethanolic solutions of $Ni(NO_3)_2$ or $NiCl_2$ were reacted with 1–3 equiv of AEAPTS (Table 2). The UV spectra did not change significantly upon gelation. This implies that the complexes $[Ni(AEAPTS)_n]^{2+}$ ($n = 1$–3) were formed, which correspond to $[Ni(en)_n]^{2+}$ or $[Ni(dbn)_n]^{2+}$. The nickel complexes were retained in the xerogels.

A different UV spectrum (absorption maximum at about 580 nm) was obtained when $Ni(acac)_2$ was equally reacted. The spectrum was the same as that reported for $Ni(acac)_2(en)$.[9] This indicates the formation of the complex $Ni(acac)_2$(AEAPTS). $Ni(acac)_2$(en) was independently prepared and its structure is shown in Fig. 1.

The same general trend was found for the other silanes used in this study. The spectra of the complexes formed with 2 equiv of APS as the complexing ligand were very similar to the corresponding complexes with 1 equiv of AEAPTS. It was therefore assumed that the same types of complexes were formed. The UV spectra of the complexes formed from $Ni(OAc)_2$, $Ni(NO_3)_2$ or $NiCl_2$ and 1 equiv of TRIAMIN analogously corresponded to that of $Ni(trien)(NO_3)_2$ (trien = triethylenediamine) ($\lambda_{max} = 374$, 602 nm),[10] while the spectrum of the complex obtained from $Ni(acac)_2$ and TRIAMIN was again different. The structure of the latter complex is unknown; it can be assumed however, that the TRIAMIN and at least one acac ligand are bonded to Ni^{2+}.

In summary, the presence of the $(RO)_3Si(CH_2)_3$ substituent had little or no influence on the coordination chemistry of the

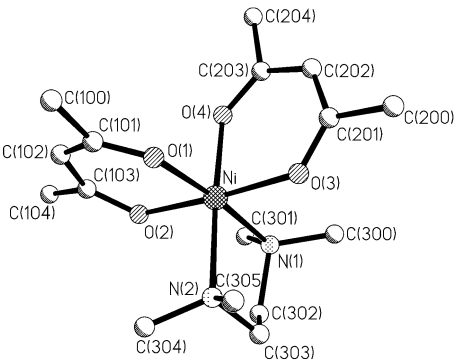

Fig. 1 Molecular structure of $Ni(acac)_2$en. Ni–O 202.9–203.7(4), Ni–N 218.0, 218.7(5) pm; O(1)–Ni–O(2) 89.0 (2), O(3)–Ni–O(4) 90.04 (14), N(1)–Ni–N(2) 83.9(2)°.

amino group(s). Coordination of the nickel ions was retained when the precursor solution was gelled, since there was nearly no change in the UV spectra compared to the solution spectra.

The results of the surface and pore analyses are given in the ESI (Table S1). Apart from the specific surface area and total pore volume calculated by the BET method, the specific pore volume and the mean pore radius calculated by the BJH method are given. The latter method does not take micropores (diameters < 1.7 nm) into consideration. In the absence of micropores, the values calculated by the BET and BJH method are the same; in the presence of micropores, the pore volume calculated by the BET method is higher. The surface and pore properties of the xerogels reported in this work depend on both the counter-ion of the employed nickel salt and the complexing silane. Since the pore volumes calculated by the BET and BJH method are about the same, the xerogels contain no micropores.

Comparison of the xerogels prepared from different metal salts (Fig. 2) shows that the surface and pore structure of the xerogels NO(X)x and Cl(X)x on one hand, and of the Ac(X)x and Acac(X)x samples on the other hand, are very similar. Both the dominant type of the adsorption isotherm and the specific surface areas and pore sizes are very similar. All NO(X)x samples and most Cl(X)x samples have type II isotherms.[11] In the Ac(X)x and Acac(X)x samples, the pore type depends on the complexing silane; when the samples are obtained as powders, the isotherms are also of type II, in the other cases the xerogels are mesoporous with type IV isotherms.

The dependence of the surface area and pore structure on the complexing silane was recently investigated for xerogels prepared from cobalt, nickel or copper acetate.[5] The observed general trends were also found in the present study (Fig. 3 and 4). In series A–C (1–3 equiv of AEAPTS), the total pore volume and the average pore radius decreased with an increasing proportion of the complexing silane when nickel acetate or acetylacetonate was employed. For example, the total pore volume of Ac(C)x (0.128 $cm^3\ g^{-1}$) is only a tenth of that of Ac(A)x (1.19 $cm^3\ g^{-1}$), and the pore radius decreases from 5.7 nm in Ac(A)x to 1.8 nm in Ac(C)x. No significant trend was found for the xerogels prepared from nickel chloride and nitrate.

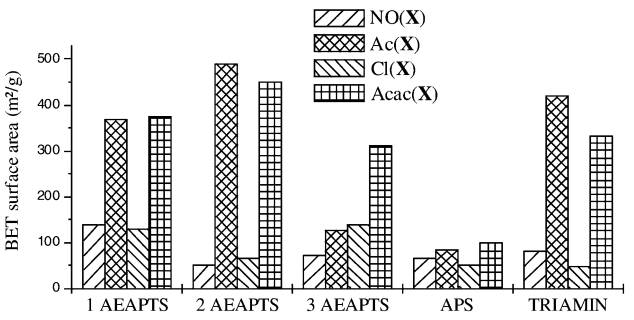

Fig. 2 BET surface areas of the xerogels (before oxidation).

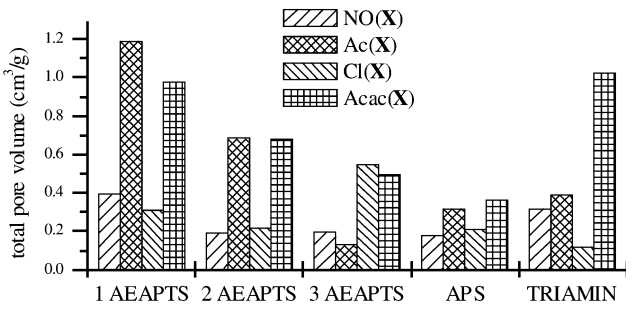

Fig. 3 Total pore volume of the xerogels (before oxidation).

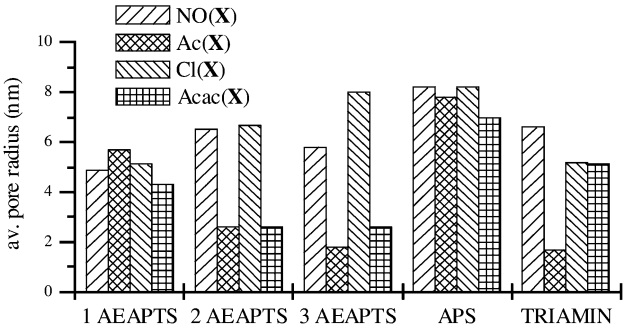

Fig. 4 Average pore radius of the xerogels (before oxidation).

All xerogels of series D (APS as the complexing silane), which are obtained as fine powders, have type II isotherms with large pore radii (7.0–8.2 nm), rather low pore volumes and small specific surface areas. The pore and structure properties of the xerogels of series E (TRIAMIN as the complexing silane) again differ strongly, depending on the employed nickel salt.

Nickel oxide/SiO_2 nanocomposites

According to thermogravimetric analyses, heating the xerogels in air to 550 °C is sufficient to remove all organic moieties (Table S2, ESI). As a general trend, the obtained xerogels NO(X) and Cl(X), which were obtained as fine powders, were rather hygroscopic and had a higher proportion of adsorbed water. The color of the xerogels was between light brown and black. Freshly prepared NiO is yellow but turned to olive-green and black when exposed to air.[12] The elemental analyses (Table S2, ESI) showed that the organic groups were nearly completely removed; the residual carbon content was in most samples clearly below 1%. The residual hydrogen values of about 1% are due to adsorbed water or Si–OH groups. Some samples prepared from $NiCl_2$ still had rather high chlorine contents after calcination (up to 2%). However, the residual chlorine was removed in the subsequent reduction step.

DSC investigation of the samples revealed two trends concerning the thermal decomposition/oxidation.

(i) Influence of the counter-ion. The samples NO(X) and Ac(X) decomposed more spontaneously and showed sharp peaks in DSC, while the Cl(X) and Acac(X) samples decomposed over a wide temperature range. Fig. 5 shows the DSC diagrams for series D, as an example. The samples of this series

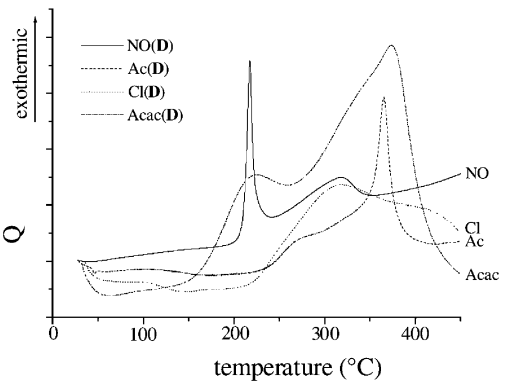

Fig. 5 DSC diagrams of series D showing the dependence of the oxidation reaction on the counter-ion.

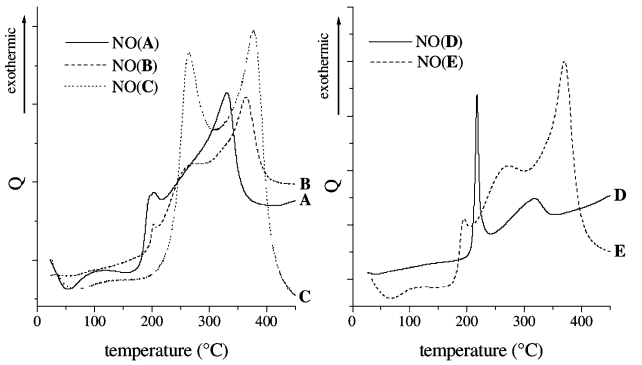

Fig. 6 DSC diagrams of the NO(X) series showing the dependence of the oxidation reaction on the kind and proportion of the complexing silane.

had a similar pore and surface structure (see below), therefore, a structural effect on the thermal decomposition can be largely excluded. NO(D) decomposed nearly explosively at about 220 °C, while Ac(D) had a sharp DSC maximum at about 365 °C. TGA of NO(D) showed that the thermal event at 220 °C corresponds to nearly 50% of the weight loss.

(ii) Influence of the complexing silane. The influence of the complexing silane on the thermal decomposition behavior is shown in Fig. 6 for the NO(X) series, as an example. The samples NO(A–C) showed that an increasing proportion of the complexing silane shifted the complete degradation of the organic groups to higher temperatures. However, comparison with the samples NO(D,E) demonstrates that not only the proportion of organic groups influences the thermal behavior, but—to a higher degree—the kind of complexing silane, that is the kind of formed metal complex. However, one should keep in mind that the samples also differ in their pore and surface structure. Both have an important influence on the heat dissipation.

In Fig. 7(a), the powder X-ray diffractograms of series B are shown, as an example. The broad hump at $2\Theta \sim 22°$ is due to amorphous SiO_2, the other reflections were assigned to bunsenite (NiO).[13] The crystallite sizes were calculated from the XRD line broadening and are given in Table 3. They depend very strongly on the counterion of the employed nickel salt. As a general trend, the NiO crystallite size increases in the order Ac(X)o < NO(X)o ≪ Acac(X)o < Cl(X)o. The nickel oxide

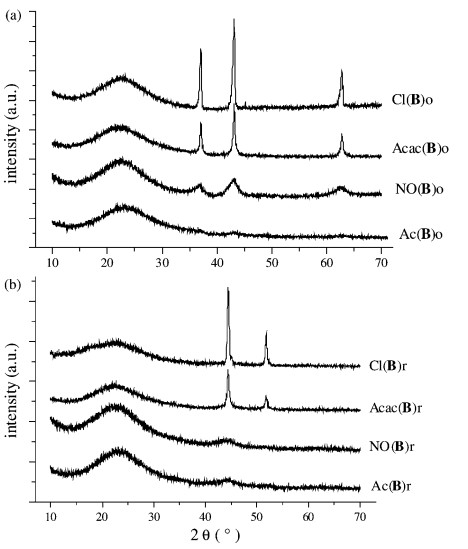

Fig. 7 Powder X-ray diffractograms of the NiO/SiO_2 (top) and Ni/SiO_2 (bottom) nanocomposites of series B.

Table 3 NiO and Ni (in brackets) crystallite diameters (in nm) calculated from the (200) reflection of the powder XRD of the composites

	Nitrate	Acetate	Chloride	Acetylacetonate
Series A	—[a] (—[a])	—[a] (—[a])	30/325[b] (82[b])	17 (10)
Series B	4.8 (—[a])	—[a] (—[a])	51 (59)	29 (15)
Series C	<3 (—[a])	—[a] (—[a])	41/114[b] (63[b])	24 (16)
Series D	—[a] (—[a])	—[a] (—[a])	357 (—[a])	20 (14)
Series E	4.9 (—[a])	—[a] (—[a])	45 (61[b])	19 (11)

[a] No reflections observed, or reflection too weak for particle size calculation. [b] Bi- or polymodal.

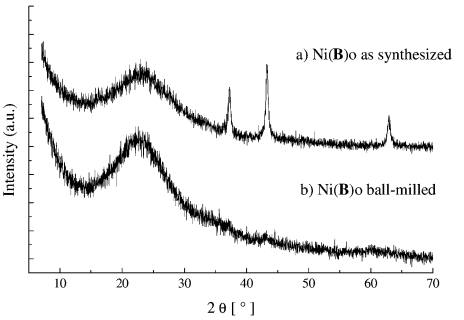

Fig. 8 Powder X-ray diffractograms of sample Ac(B)o: (a) as obtained after drying and (b) after ball-milling.

particles in the samples prepared from $Ni(NO_3)_2$ and, in some cases, from $Ni(OAc)_2$, were obviously amorphous or (more likely) too small (below ~3 nm) to give a XRD pattern. Some of the Cl(X)o samples contained rather big particles.

It turned out to be essential to grind the solid masses in a ball mill before calcination to get reproducible results and small metal particles after calcination and reduction. This is shown in Fig. 8 for samples similar to Ac(B)o (with 50% higher nickel content) after calcination. Both samples were calcined under the same conditions, the upper sample in Fig. 8 as obtained after drying (with irregular grain sizes in the mm range), while the lower was ball-milled before (grain size in the μm range). While in the untreated sample the diffraction pattern of bunsenite (NiO) can be clearly identified and an average particle size of 25 nm was calculated from the line width, the NiO particles in the ball-milled samples were too small (<3 nm) to give sufficiently intense XRD signals. We interpret this finding by the following argument: the heat generated during (exothermic) burning of the organic groups cannot be dissipated fast enough when the sample is too compact. This may lead to local over-heating and thus to extensive growth of NiO

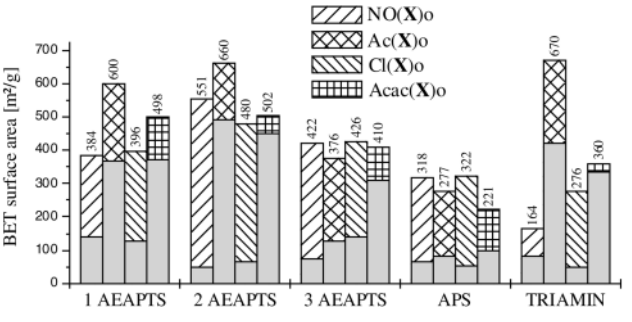

Fig. 9 Comparison of the BET surface areas before and after the oxidation step. For each sample, the smaller shaded bar is the surface area before oxidation.

particles. Another explanation is that nucleation centers are created by ball-milling, which lead to smaller crystallites.

Upon calcination of the xerogels, the specific surface area of the samples increased strongly (Fig. 9) with concomitant decrease of the mean pore radii (Table S1, ESI). Both phenomena are due to the removal of the organic groups, which creates new pores. A comparison of the BET and BJH values in Table S1 shows that, in most cases, part of the new pores were micropores. In most samples, the total pore volume increased upon calcination, as expected. However, in the Acac(X) series, the total pore volume decreased; additionally, the relative increase in surface area in this series was smaller than in the other series (Fig. 9). We have currently no explanation for this surprising result.

Nickel/SiO_2 nanocomposites

The calcined samples were reduced by hydrogen at 500 °C. The color of the reduced samples was between dark brown and black. Elemental analyses of the Cl(X)r series (as an example) showed that the residual chlorine was removed during the reduction step (Table S3, ESI). Nickel analyses of selected samples gave distinctly smaller values than the theoretical 8.5% [found, for NO(B)r 5.29%, Cl(C)R 7.62%, Acac(D)r 6.84%, NO(E)r 6.60%], that is, 10–38% nickel was lost during calcination and reduction. The most probable explanation is that volatile nickel carbonyl was formed during calcination.

In Fig. 7(b), the powder X-ray diffractograms of series B are shown, as an example. The observed reflections are those of elemental nickel,[14] and no reflections of NiO are observed, meaning that at least the crystalline proportions of the incorporated nickel are completely reduced. The calculated nickel particle diameters are given in Table 3. In all samples of the NO(X)r, and Ac(X)r series, the reflections of elemental nickel were too weak for the size determination. In the samples of the Acac(X)r series, the nickel particles were on the average about 30% smaller than the NiO particles in the corresponding Acac(X)o series. This size reduction has probably two reasons: (i) the unit cell volume of Ni is about 60% that of NiO, that is the particles shrink upon reduction; (ii) the Ni particles may be covered by an amorphous nickel oxide or nickel silicate layer.[1d] It can nevertheless be concluded that the reduction step resulted in neither re-dispersion nor in particle growth.

In the Cl(X)r series [as in the Cl(X)o samples], a realistic calculation of the particle size is difficult, because most samples have a bimodal size distribution. In an earlier study,[1b] we also found a bimodal size distribution in the TEM investigation of samples prepared from $Ni(OAc)_2$ and AEAPTS, but only when the nickel proportion exceeded 14 wt %. In studies with different metals, we found a bimodal size distribution only for nickel as the metal component, and in combination with only some counter-ions.[1b,d] We currently cannot explain this phenomenon; it may be due to transport phenomena occurring in the matrix during calcination and/or reduction.

The general appearance of the adsorption isotherm and the pore volumes did not change significantly in the reduction step (Table S1, ESI). In same cases, particularly in series D, the specific surface area decreases somewhat. This is probably due to relaxation phenomena caused by the heating during reduction.

Highly dispersed nickel on a pre-formed silica support

One of the advantages of the sol-gel method of preparing highly dispersed metal particles is that solid supports can be coated with the sols containing the tethered metal complexes.[3] In the present study, sols prepared from $[(RO)_3Si(CH_2)_nA]_nNiX_m$ precursors were used to impregnate silica spheres. No TEOS was added to the precursor solution. Formation of the metal oxide particles by calcination and metal particles by reduction then occurred on the support. The amount of the employed nickel salt was chosen to give a nickel loading of about 8–8.5 wt %. This value refers to the to the total mass, that is the outer layer on the silica spheres may be richer in metal than the center although the cross-section of the metal-loaded spheres had a homogeneous appearance to the naked eye.

Table 4 Nickel analysis of the impregnated silica spheres (theoretical values in brackets)

	$Ni(NO_3)_2$	$Ni(OAc)_2$	$NiCl_2$	$Ni(acac)_2$
1 AEAPTS	8.5 (8.22)	8.4 (8.26)	8.4 (8.23)	8.4 (8.45)
2 AEAPTS	8.5 (7.92)	8.2 (8.04)	7.8 (7.87)	—
3 AEAPTS	9.1 (8.02)	8.2 (7.98)	8.5 (7.89)	8.5 (8.04)
2 APS	8.5 (8.34)	8.5 (8.27)	8.2 (8.21)	8.5 (8.56)
1 TRIAMIN	8.5 (8.46)	7.7 (8.19)	8.5 (8.51)	8.5 (8.50)

Table 5 NiO and Ni (in brackets) crystallite diameters (in nm) calculated from the (111) reflection of Ni on the silica spheres containing 8.5 wt % nickel

	Nitrate	Acetate	Chloride	Acetylacetonate
Series A	7[a] (5)	—[b] (—[b])	19 (16)	8[a] (8)
Series B	5[a] (8)	15 (17)	18 (15)	—
Series C	5 (6)	15 (17)	17 (18)	17 (18)
Series D	3 (4)	12 (9)	24 (24)	11[a] (10)
Series E	8[a] (—[b])	—[b] (—[b])	28[a]	13[a] (—[b])

[a] Calculated from the (200) reflection. [b] No reflections observed, or reflection too weak for particle size calculation.

The specific surface areas and pore radii of the loaded spheres decreased only slightly compared with the unloaded spheres. For example, the surface area of the spheres loaded with system Ac(C) was 326 m^2 g^{-1} after calcination, with a mean pore diameter of 5.4 nm (unloaded spheres: BET surface area 376 m^2 g^{-1}, pore diameter 7.8 nm). The shape of the nitrogen adsorption/desorption hysteresis was also very similar.

Contrary to the xerogel powders described above, there was nearly no loss of nickel during the oxidation and reduction step for the loaded silica spheres. The nickel content of the reduced samples was nearly as calculated (Table 4). A possible explanation for this phenomenon is that volatile nickel compounds (nickel carbonyl, for example) are more easily carried out of the system when the powder particles are small. In the pores of the bigger silica spheres volatile compounds may be decomposed before they can escape into the ambient gas phase.

The nickel particle size after reduction is given in Table 5. Nickel nitrate gives the smallest particles and nickel chloride the largest, rather independent of the complexing silane. However, the size differences are much smaller than in the composite powders, and there are no bimodal size distributions for the $NiCl_2$ derived particles. It appears that the silica pellets have a leveling effect on the particle sizes.

Conclusions

Different methods have been used to prepare nickel dispersions in sol-gel materials: impregnation of porous xerogels by metal salt solutions, addition of metal compounds to the sol or to the precursor solution before gelling, or tethering of metal complexes to functionalized metal alkoxides.

A general observation is that anchoring the metal ion to the matrix during network formation favors high nickel dispersions in silica. In the approach described in this work, nickel complexes, formed *in situ* from nickel salts and amino-substituted organotrialkoxysilanes, were employed. However,

any other kind of tethering the metal to the gel network may be equally successful to obtain small nickel particles.[15]

In the present work, two types of nanocomposite materials were prepared, both containing about 8–8.5 wt % elemental nickel: (i) Ni/SiO_2 nanocomposite powders obtained by sol-gel processing of $[(RO)_3Si(CH_2)_nA]_nNiX_m$–$Si(OR)_4$ precursor mixtures, followed by calcination to remove the organic groups and reduction of the initially obtained nickel oxide particles. In these materials, the silica matrix is mainly formed from $Si(OR)_4$. (ii) In the second group of materials, pre-formed silica spheres were used as a support, which were impregnated by a sol obtained from $[(RO)_3Si(CH_2)_nA]_nNiX_m$.

In both cases, the nickel particle size is nearly independent of the kind and proportion of the complexing ligand in the precursor mixture. However, it depends on the counter-ion of the employed nickel salt. This result is in contrast to our previous investigations on Pt/SiO_2, where a dependence of the average platinum particle diameter on *both* the counter-ion of the employed platinum salt and the complexing silane was found.[3] The particle size variations due to the different counter-ions are much smaller for the impregnated spheres than for the composite powders.

The smallest Ni crystallites (<3 nm) were obtained when nickel nitrate (also nickel acetate for the powders) was employed as the metal salt both for the nanocomposite powders and the coated silica spheres. Larger nickel particles were formed from nickel acetylacetonate. This possibly reflects the fact that a different kind of metal complex was obtained due to the retention of coordination of the acac ligands. Nickel chloride gave large particles, especially in the powdery materials, where additionally bimodal size distributions were obtained. We attribute this different behavior to facilitated transport of halogenated nickel species either *via* the gas phase or *via* the inner silicate surface.

At this point, a comparison with the conventional sol-gel approach to prepare nickel particles in silica is appropriate. Nickel particles with 6–8 nm diameter were obtained by gelling $Si(OEt)_4$ in the presence of $Ni(NO_3)_2$ (acid catalysis) without a complexing silane.[16] When the nickel ions of $Ni(NO_3)_2$ are coordinated by amino-substituted organotrialkoxysilanes, the resulting nickel particles are significantly smaller. However, when other nickel salts are used, such as $Ni(acac)_2$, the metal particles are larger than for $Ni(NO_3)_2$ without a complexing silane. This comparison demonstrates that tethering of the metal ions to the gel matrix during sol-gel processing is a necessary but not sufficient condition to obtain small metal particles with narrow size distributions.

A possible role of the counter-ion on the metal particle size may be its thermal decomposition behavior, which possibly influences the particle growth during the calcination step. Our DSC investigations showed that the thermal decomposition/oxidation of the nitrate- and acetate-containing samples is characterized by exothermic thermal events in a small temperature range, while the chloride- and acetylacetonate-containing samples decompose over a wide temperature range. Our hypothesis is that the local heat generated by a sudden exothermic event is dissipated before it affects the growth of the metal particles. When the heat is generated over a wider temperature range, it promotes diffusion of nickel species and thus particle growth to a much higher degree.

An indirect effect of the organic moieties may be that they influence the texture of the silica matrix. From the surface and pore analysis data (Table S1, ESI) it is obvious that different gel morphologies are obtained depending on the complexing silane/counter-ion combination. Although the specific surface area increases upon calcination, the general pore type is retained during calcination and reduction. A different pore and surface structure of the gels may dissipate the local heat generated by the pyrolysis/oxidation of the organic groups more or less efficiently.

The results obtained for the impregnated silica spheres strongly support the hypothesis that the morphology of the silica matrix has a strong effect on the metal particle size. It can be assumed that the overall morphology of the silica spheres is not greatly changed during the early preparation steps, that is the heat dissipating influence of the silica matrix should be very similar for all samples. A leveling effect of the pre-formed silica matrix on the nickel particle size was indeed observed. It can be concluded that the creation of somewhat different gel structures by the employed complexing silane/counter-ion combinations is the main reason for the observed variations of the nickel particle sizes. Nevertheless, there also appears to be some influence of the different thermochemistry.

Experimental

Tetraethoxysilane (TEOS, Merck), *N*-(aminoethyl)aminopropyltrimethoxysilane (AEAPTS, Wacker), {*N*[(*N*-aminoethyl)-aminoethyl]aminopropyl}trimethoxysilane (TRIAMIN, Geleste), aminopropyltriethoxysilan (APS, Wacker), $Ni(OAc)_2 \cdot 4H_2O$ (Aldrich), $NiCl_2 \cdot 6H_2O$ (Aldrich) $Ni(NO_3)_2 \cdot 6H_2O$ (Aldrich) and $Ni(acac)_2$ (96%, Acros) were used as received. The used ethanol was water-free and not denatured. The silica spheres (Riedel de Haen Kieselgel 60) had diameters of 0.2–0.5 mm, a BET surface area of 376 $m^2 \cdot g^{-1}$ and pores with a diameter of 7.8 nm. All operations were carried out in air if not otherwise stated.

UV-Vis spectra were recorded on a Perkin Elmer Lambda 15 spectrometer; the data were handled with the program UV-WinLab 2.70. The spectra of solid samples were recorded with a $BaSO_4$ reflection sphere.

Thermal analyses were performed on Shimadzu TGA-50 and DSC-50, and nitrogen physisorption experiments on an ASAP 2010 (Micromeritics) at −196 °C in the p/p_0 range 0.01–1 (50–55 data points). The metal-complex-containing xerogels were degassed at 80 °C/10 mTorr, and the metal oxide or metal-containing samples at 250 °C/10 mTorr. The specific surface areas and total pore volumes were calculated according to the BET method. The specific pore volume and the mean pore radii were calculated from the adsorption isotherm for pores with diameters of 1.7–300 nm according to the BJH method.

The X-ray diffractograms were recorded with Cu-K_α radiation on a Phillips PW 1710 diffractometer. The average metal and metal oxide particle sizes were calculated from the strongest reflection [NiO(200) = 2.088 ($2\theta = 47.5°$); Ni(111) = 2.034 ($2\theta = 44.5°$)] by the Debye–Scherrer equation. The peaks were approximated by a Gaussian function without correction, assuming a symmetric peak profile.

Preparation of xerogel powders

The nickel salt (1.45 mmol) was dissolved in 100 ml of ethanol. After addition of the amino-substituted silane, the solution was stirred at room temperature until the metal salt was completely dissolved. The suspension containing $Ni(acac)_2$ had to be refluxed for several hours. Then an amount of 0.2 N aqueous ammonia was added that corresponded to a 7.5-fold excess of water relative to all alkoxy groups from TEOS and the amino-substituted silane. A calculated amount of TEOS was added after 15 min. Exact quantities of all reagents are given in Table S4 in the ESI. Then the temperature was raised to 70 °C and held for 3 days after which the solvent was evaporated. The obtained solids were dried at 80 °C/0.1 Torr.

X-Ray structure analysis of $Ni(acac)_2$en

A crystal was mounted on a Siemens SMART diffractometer with a CCD area detector. Graphite-monochromated Mo-K_α

radiation (71.073 pm) was used for all measurements. The crystal-to-detector distance was 4.40 cm. A hemisphere of data was collected by a combination of three sets of exposures at 293 K. Each set had a different ϕ angle for the crystal, and each exposure took 20 s and covered 0.3° in ω. The data were corrected for polarization and Lorentz effects, and an empirical absorption correction (SADABS) was applied. The cell dimensions (monoclinic, space group *Pn*, $a = 850.48(3)$, $b = 1021.19(4)$, $c = 1152.20(4)$ pm, ß = 92.241(1)°, $Z = 2$) were refined with all unique reflections. The structure was solved by direct methods (SHELXS86). Hydrogen atoms were inserted in calculated positions and refined riding with the corresponding atom. Refinement was carried out with the full-matrix least-squares method based on F^2 (SHELXL93) with anisotropic thermal parameters for all non-hydrogen atoms ($R_1 = 0.048$, $R_2 = 0.123$) using all 2612 independent reflections.

CCDC reference number 184381. See: http//www.rsc.org/suppdata/nj/b1/b110612k/ for crystallographic data in CIF or other electronic format.

Calcination of the xerogel powders

The xerogels were ground in a ball mill for 15 min and then placed in a ceramic boat. The boat was placed in a muffle furnace, heated to 550 °C in air at a rate of 10 °C min^{-1} and then held at 550 °C for 30 min. The weight loss and elemental analyses are given in Table S2 (ESI).

Reduction of the nickel oxide/silica composites

The calcined samples were placed in a ceramic boat. The boat was placed in a horizontal quartz tube, heated to 500 °C in hydrogen (200 ml·min^{-1}) at a rate of 10 °C min^{-1}, then held at 500 °C for 3 h and then slowly cooled to 100–150 °C under hydrogen. The final cooling to room temperature was done under argon. Elemental analyses of selected samples are given in Table S3 (ESI).

Preparation of Ni particles on a silica support

The nickel salt (3.3 mmol) was dissolved in 100 ml of warm ethanol. Then the calculated amount of AEAPTS (the tri-*ethoxy* derivative) or APS was added and the solution was stirred for 15 min. No TEOS was added to keep the metal concentration high and to prevent agglomeration of the spheres. Then an amount of 0.2 N aqueous ammonia (7.5-fold excess relative to all alkoxy groups) was added and the calculated amount of silica spheres (corresponding to 8.5 wt % elemental Ni in the final material). The exact amounts of all reagents are given in Table S5 of the ESI. The mixture was stirred for 5 min at room temperature and then the solvent was removed *in vacuo*. The loaded spheres were dried at 70 °C and 12 Torr for 3 h.

The dried samples were placed in a horizontal quartz tube, heated to 550 °C at a rate of 10 °C min^{-1} under a stream of air (200 ml min^{-1}) and then held at 550 °C for 30 min. Reduction was carried out by passing hydrogen (200 ml·min^{-1}) over the sample at 500 °C for 3 h. The reduction period was extended to 10 h for one sample. There was no change of the line widths in the XRD spectra, that is the metal particles did not sinter under these conditions.

References

1 (*a*) U. Schubert, S. Amberg-Schwab and B. Breitscheidel, *Chem. Mater.*, 1989, **1**, 576; (*b*) B. Breitscheidel, J. Zieder and U. Schubert, *Chem. Mater.*, 1991, **3**, 559; (*c*) U. Schubert, B. Breitscheidel, H. Buhler, C. Egger and W. Urbaniak, *Mater. Res. Soc. Symp. Proc.*, 1992, **271**, 621; (*d*) W. Mörke, R. Lamber, U. Schubert and B. Breitscheidel, *Chem. Mater.*, 1994, **6**, 1659; (*e*) U. Schubert, F. Schwertfeger and C. Görsmann, *ACS Symp. Ser.*, 1996, **622**, 366.

2 (*a*) C. Görsmann, U. Schubert, J. Leyrer and E. Lox, *Mater. Res. Soc. Symp. Proc.*, 1996, **435**, 625; (*b*) U. Schubert, C. Görsmann, S. Tewinkel, A. Kaiser and T. Heinrich, *Mater. Res. Soc. Symp. Proc.*, 1994, **351**, 141; (*c*) A. Kaiser, C. Görsmann and U. Schubert, *J. Sol-Gel Sci. Technol.*, 1997, **8**, 795.

3 C. Lembacher and U. Schubert, *New J. Chem.*, 1998, **22**, 721.

4 (*a*) B. Heinrichs, F. Noville and J.-P. Pirard, *J. Catal.*, 1997, **170**, 366; (*b*) B. Heinrichs, P. Delhez, J.-P. Schoebrechts and J.-P. Pirard, *J. Catal.*, 1997, **172**, 322.

5 G. Trimmel and U. Schubert, *J. Non-Cryst. Solids*, 2001, **296**, 188.

6 T. Ueckert, R. Lamber, N. I. Jaeger and U. Schubert, *Appl. Catal., A*, 1997, **155**, 75.

7 G. A. Martin, *J. Catal.*, 1979, **60**, 452.

8 D. L. Leussing, J. Harris and P. Wood, *J. Phys. Chem.*, 1962, **66**, 1544.

9 K. Dey and S. K. Sen, *J. Indian Chem. Soc.*, 1977, **54**, 477.

10 N. F. Curtis and Y. M. Curtis, *Inorg. Chem.*, 1965, **4**, 804.

11 K. S. Sing, D. H. Everett, R. A. W. Aul, L. Moscou, R. A. Pierotti, J. Rouquerol and T. Siemieniewska, *Pure Appl. Chem.*, 1985, **57**, 603.

12 *Handbuch der präparativen anorganischen Chemie*, ed. G. Brauer, Enke, Stuttgart, Vol. 3, 1981.

13 *JCPDS Data File*, 1996, entry no. 04-0835.

14 *JCPDS Data File*, 1996, entry no. 04-850.

15 A recent example: S. Dirè, R. Ceccato, G. Facchin and G. Carturan, *J. Mater. Chem.*, 2001, **11**, 678.

16 (*a*) G. Ennas, A. Mei, A. Musinu, G. Piccaluga, G. Pinna and S. Solinas, *J. Non-Cryst. Solids*, 1998, **232–234**, 587; (*b*) G. Ennas, A. Falqui, G. Piccaluga, S. Solinas, D. Gatteschi and C. Sangregorio, *Z. Naturforsch. A*, 2000, **55**, 581.